Journal of Radiation Research and Applied Sciences 17 (2024) 100885

Contents lists available at ScienceDirect

Journal of Radiation Research and Applied Sciences

journal homepage: www.journals.elsevier.com/journal-of-radiation-research-and-applied-sciences

Breast cancer classification method based on improved VGG16 using mammography images☆

Zhaoqi Liu [a], Jidong Peng [a], Xiumei Guo [b], Shaoqiong Chen [b], Liansheng Liu [b,*]

[a] Department of Radiology, Ganzhou People's Hospital, Ganzhou, Jiangxi Province, 341000, China
[b] Department of Medical Imaging, The Sixth Affiliated Hospital of Jinan University, Dongguan Eastern Central Hospital, Dongguan, Guangdong Province, 523576, China

ARTICLE INFO

Keywords:
Breast X-ray mammography image classification
Convolutional neural network
Imbalanced data
Transfer learning
Data augmentation

ABSTRACT

Background and objective: Breast cancer has become the leading global cancer, and early detection and diagnosis of breast cancer are of paramount importance for treatment.
Methodology: This paper proposes a breast X-ray mammography image classification model based on Convolutional Neural Network (CNN). The model categorizes breast X-ray mammography images into benign and malignant classes. Built upon the VGG network, the model adjusts the network structure and conducts experiments on the dataset collected and organized by the Medical Imaging Department of Ganzhou People's Hospital and The Sixth Affiliated Hospital of Jinan University. To address the issue of imbalanced data in the dataset, the model employs a focal loss function for optimization and combines transfer learning and data augmentation strategies during network training.
Results: Experimental results demonstrate that the model achieves an average recognition rate of 96.945% across four different magnification levels. Notably, recognition rates exceed 95.5% for the 50X, 100X, and 200× magnification levels, demonstrating excellent classification capabilities.
Conclusion: This model ignificantly improving classification accuracy compared to previous models, which provides meaningful insights into the classification of breast X-ray mammography images.

1. Introduction

According to the International Agency for Research on Cancer (IARC) of the World Health Organization (WHO) in 2020, breast cancer has officially surpassed lung cancer, becoming the leading global cancer (Wild et al., 2020). Among cancer patients, breast cancer has the highest prevalence among females, far surpassing other types of cancer. Currently, the primary method for diagnosing breast cancer relies on histopathological analysis. The final diagnosis, including grading and staging, is mostly derived from the analysis of histopathological images by pathologists, making it the gold standard for diagnosing breast cancer (Spanhol et al., 2016a).

In recent years, advancements in medical imaging and artificial intelligence have revolutionized healthcare. Breast X-ray imaging analysis offers new avenues for early detection (Zhao et al., 2023), cardiovascular segmentation enhances cardiac (Wong et al., 2022), ultrasound imaging aids in precise diagnostics (Zhu et al., 2020), and lung nodule segmentation improves pulmonary disease assessment (Shi et al., 2021a). Pulmonary image super-resolution reconstruction enhances image clarity and interpretation (Shi et al., 2021b), medical and health big data management streamlines patient records and research (Ye et al., 2021), and machine learning and artificial intelligence are transforming medical decision support systems (Wong et al., 2012, 2020). These developments collectively contribute to improved diagnostic accuracy and healthcare efficiency.

With the advancement of computer technology, many researchers have attempted to apply Computer-Aided Diagnosis (CAD) in the automatic classification of breast mammography images, achieving significant progress. In the traditional field of machine learning, the methods for automatic diagnosis are mainly based on manual feature extraction, combined with classifiers. Roy et al. (Roy et al., 2021) designed feature extractors that extracted texture and statistical features, combining these features to create a dataset with 782 features. They achieved an optimal recognition rate of 92.55% by training and classifying using various classifiers. Spanhol et al. (Spanhol et al., 2016a) released the BreakHis dataset and used six different feature extractors on this dataset.

☆ Basic Research Program of Guangzhou Science and Technology Bureau in 2024, jointly funded by Guangzhou and Jinan University (No: 2024A03J0152).
* Corresponding author.
E-mail address: llsjnu@sina.com (L. Liu).

https://doi.org/10.1016/j.jrras.2024.100885
Received 30 October 2023; Received in revised form 21 February 2024; Accepted 12 March 2024
Available online 25 March 2024

They combined four classifiers for each feature extractor, resulting in recognition accuracies ranging from 80% to 85%. However, manual feature extraction is not only time-consuming and labor-intensive but also requires feature extractors to possess relevant domain knowledge. Additionally, the experience and mental state of feature extractors can significantly impact the quality of feature extraction, hindering the practical application of computer-aided diagnostic technology.

In recent years, with the rapid development of computer processing power and artificial intelligence, deep learning technology has found significant applications in various fields, especially in image processing (LeCun et al., 2015). Deep learning technology allows for automatic feature extraction from images, eliminating the limitations of manually extracting features in traditional machine learning and saving human effort. Many researchers have applied deep learning technology to breast cancer diagnosis, to some extent improving the accuracy of breast cancer diagnosis. Spanhol et al. (Spanhol et al., 2016b) applied AlexNet network to the BreakHis dataset, achieving an identification rate 6% higher than traditional machine learning algorithms. Nawaz et al. (Nawaz et al., 2018) used the DenseNet CNN model to predict subtypes of breast tumors with an accuracy of 95.4%. Zou Wenkai et al. (Zou et al., 2020) adjusted the Inception structure in GoogleNet and adopted a unified training method with all magnification factors to evaluate the model at the patient level, achieving an accuracy of 87%–90%. While these methods have demonstrated certain levels of accuracy, there is still room for improvement in recognition accuracy and model robustness.

To address these issues, this study is based on the VGG16 network, with adjustments made to the network structure. Additionally, data augmentation and transfer learning strategies are employed. The trained model is used for benign and malignant classification of breast mammography images. To tackle the issue of imbalanced samples in the dataset, this study uses the Focal Loss function as the experimental loss function, which mitigates the problem of sample imbalance to some extent. The model is trained on images with four different magnification factors, enabling it to learn deeper and more complex features, thereby improving model robustness. During testing, images with different magnification factors are independently evaluated, better simulating the classification of breast cancer mammography images in real-world scenarios.

2. Materials and methods

2.1. Convolutional neural network

In the ImageNet Image Classification Competition of 2012, the AlexNet network emerged as the champion, outperforming other models of that time by a significant margin. This victory brought widespread attention to deep learning technology. In comparison to traditional machine learning methods, the advantage of deep learning lies in its ability to learn features from data without the need for manual feature extraction. This enhances both the convenience and accuracy of feature extraction. Convolutional Neural Networks (CNNs), one of the most commonly used deep learning models, have demonstrated excellent performance in the field of image processing. This study employs CNNs to construct an image classification model.

A CNN typically comprises input layers, convolutional layers, pooling layers, and fully connected layers, as illustrated in Fig. 1. When 2D or 3D images are input, convolutional layers extract features from the images, while pooling layers reduce the dimensionality and compress the data and the number of parameters. Through a series of convolution and pooling operations, CNNs can simultaneously learn low-level and high-level features of the data. In the fully connected layers, the network obtains distinguishable features that facilitate subsequent classification.

Compared to traditional neural networks, CNNs possess two significant advantages: local connectivity and weight sharing. Local connectivity is in contrast to full connectivity, where every node in the network is connected. In practice, pixel points in images tend to have stronger associations with nearby pixel points than with distant ones. Local connectivity allows the formation of highly discriminative local features. Weight sharing involves using the same convolutional kernel for convolution operations across the entire image, reducing the number of parameters and speeding up computation.

These advantages make CNNs highly effective in image classification tasks and contribute to their widespread use in various deep learning applications.

2.2. Transfer learning

Transfer learning is the process of applying knowledge gained from one task to another. Currently, there are several methods of transfer learning, including instance transfer, feature transfer, parameter sharing transfer, and relational knowledge transfer (Weiss et al., 2016).

In this study, the parameter transfer method is employed. This approach involves initializing the network with a model that has been pre-trained on another dataset (the source domain) and then fine-tuning the model on the dataset used in this study (the target domain). When training a convolutional neural network (CNN) from scratch, the parameters are typically randomly initialized. If the training dataset is small, this random initialization can lead to difficulties in learning the data patterns, potentially affecting the model's performance. By leveraging transfer learning techniques, it is possible to shorten training time, effectively mitigate underfitting and overfitting, and enhance the model's generalization performance.

The ImageNet dataset is a large-scale visual dataset for computer vision, containing over 10 million natural images categorized into 1000 classes with manual annotations (Russakovsky et al., 2015). In this study, the ImageNet dataset serves as the source domain. The network model is initially trained on this dataset, and the learned model parameters are used to initialize the network when training on the dataset specific to this study. Given the differences between natural images and medical images, this study only uses the source domain's model parameters for network initialization. Additionally, a new fully connected layer is constructed, and all parameters in the network layers are retrained and adjusted on our dataset.

2.3. VGG16 network

The VGG network was developed collaboratively by researchers from the University of Oxford's Visual Geometry Group (VGG) and Google DeepMind. It achieved second place in the classification task of the ILSVRC 2014 competition and demonstrated strong feature extraction capabilities (Simonyan & Zisserman, 2014). In this study, the classic VGG16 network serves as the foundation, with adjustments made to the

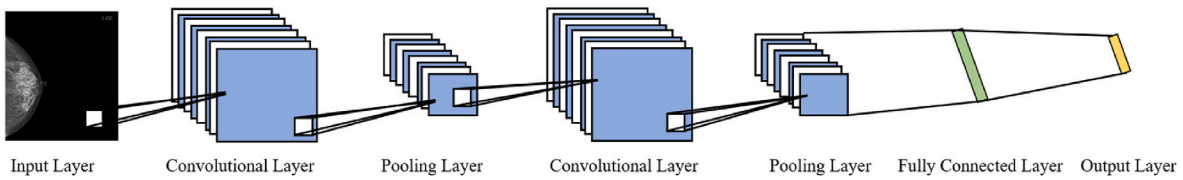

Fig. 1. Structure of a convolutional neural network (CNN).

fully connected layers. The modified network structure is illustrated in Fig. 2.

The network takes breast X-ray mammography images with dimensions of 224x224 as input and includes 13 convolutional layers, 5 max-pooling layers, and 3 fully connected layers. The number of neurons in the three fully connected layers is adjusted to 256, 128, and 2, respectively, while the original network's fully connected layers have 4096, 4096, and 1000 neurons. The adjusted VGG16 network exhibits the following characteristics.

(1) Use of Small Convolutional Kernels: The network primarily uses 3x3 convolutional kernels. Compared to larger kernels like 5x5 or 7x7, smaller kernels not only require less computation but also excel at capturing fine details in images.
(2) Reduced Number of Neurons in Fully Connected Layers: As most of the parameters in a convolutional neural network (CNN) are concentrated in the fully connected layers, compressing the dimensions of these layers can lead to a lightweight model and reduce the risk of overfitting.

One drawback of deep learning algorithms is that they can be challenging to train, often requiring significant time and being prone to getting stuck in local optima when using gradient descent. To address these issues, this study incorporates the Batch Normalization (BN) algorithm into the network. BN helps reduce the distribution gap between each training batch, accelerating network training. The formulas for the BN algorithm are shown in Equations (1) and (2):

$$\hat{x}^i = \frac{x^i - E[x^i]}{\sqrt{Var(x^i)}} \tag{1}$$

The equations presented for Batch Normalization (BN) involve the following variables: $\hat{x}^i$ represents the normalized results of all neurons' output data in the ith layer, x^i denotes the output data of neurons in the ith layer, and $E[x^i]$ and $Var(x^i)$ represent the mean (average) and variance (standard deviation squared) of the output data in the ith layer, respectively. These equations illustrate the fundamental calculations in BN, a technique used to enhance the training stability and efficiency of deep neural networks by normalizing intermediate representations during the training process.

$$\hat{y}^i = \gamma^i \hat{x}^i + \beta^i \tag{2}$$

In the provided context, $\hat{y}^i$ represents the output of the Batch Normalization (BN) layer in the ith layer, while γ^i and β^i are learnable parameters introduced by the BN algorithm. These two parameters introduce a linear transformation to neurons, allowing them to adjust their activation values.

In summary, this study utilizes a network with fewer parameters, fast training speed, and excellent classification performance.

2.4. Dataset and data Preprocessing

2.4.1. Data source

This study utilizes a dataset collected from breast X-ray mammography images obtained by the Medical Imaging Department of Ganzhou People's Hospital, Medical Imaging Department of The Sixth Affiliated Hospital of Jinan University. The dataset comprises 7909 annotated images from 91 patients, including 2393 images of benign tumors and 5448 images of malignant tumors. Each image is available in four different magnifications (50×, 100x, 200x, 400x), with dimensions of 700x460 pixels. It's important to note that these images are in grayscale, as they are two-dimensional and lack RGB color channels. Some sample images from this dataset are shown in Fig. 3, and detailed distribution information is provided in Table 1.

2.4.2. Data Preprocessing

The dataset we used contains a total of 7841 breast X-ray mammography images, which is insufficient for training neural networks. Therefore, data augmentation techniques are necessary to increase the training data, reduce the risk of model overfitting, and improve its generalization performance. Common data augmentation methods include flipping, rotation, cropping, translation, adding Gaussian noise, and applying blur.

In this study, the original dataset was split into a training set and a test set in a 7:3 ratio, and data augmentation was applied to the training set using six different transformations. Firstly, the training set data was horizontally flipped, vertically flipped, and rotated by 90°, 180°, and 270°, resulting in a six-fold increase in the amount of data. Additionally, the images were resized by a factor of 0.8 after the aforementioned transformations. As a result, the augmented training dataset was expanded to 12 times its original size, with 66110 training images and 2340 test images. The distribution of the augmented dataset is summarized in Table 2.

2.5. Training strategy

To improve the training of the classification model, the parameters of the model in this study are initialized using a transfer learning strategy.

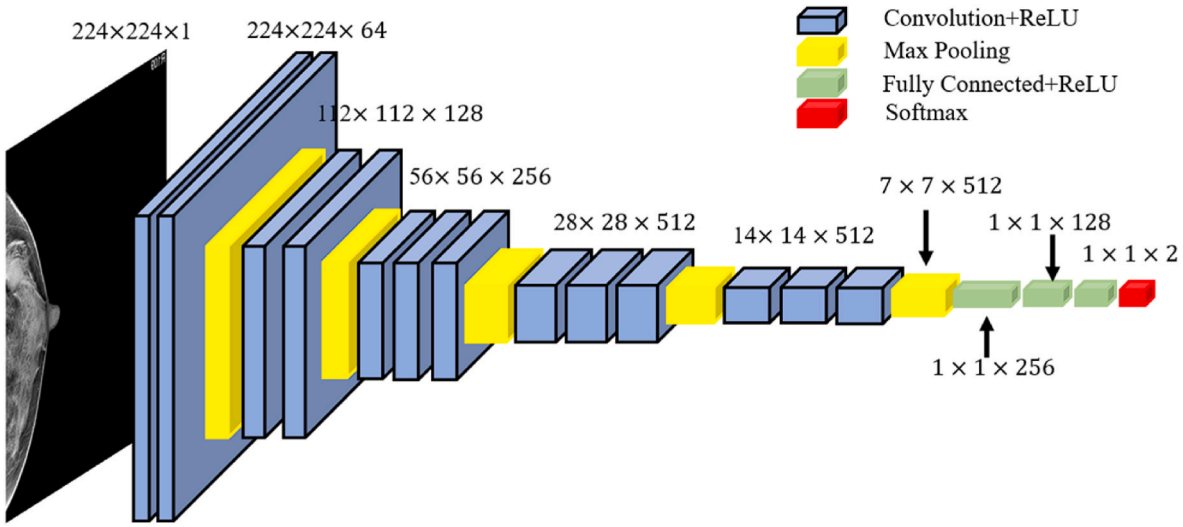

Fig. 2. Adjusted structure of the VGG network.

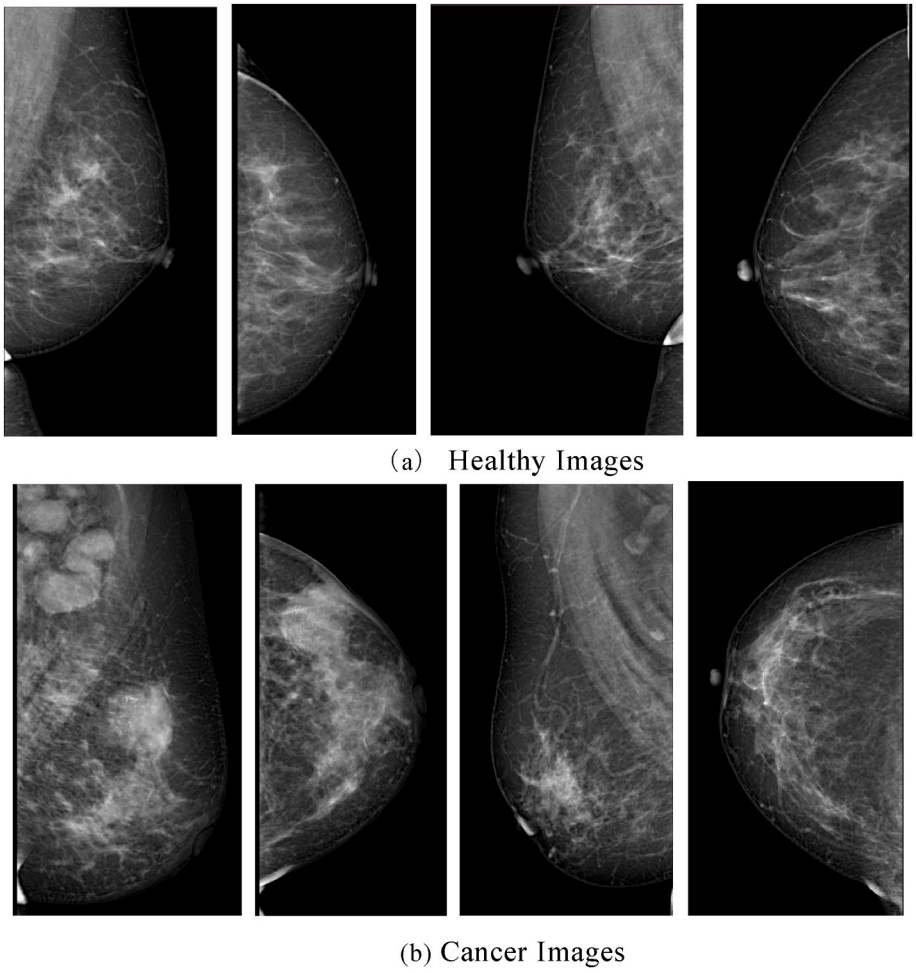

Fig. 3. (a) Healthy images
Fig. 3(b) Cancer images.

Table 1
Image distribution of benign and malignant tumors with different magnifications.

Magnification times	Healthy	Cancer	Aggregate
50X	591	1424	2015
100X	613	1389	2002
200X	587	1370	1957
400X	602	1265	1867
Aggregate	2393	5448	7841

Table 2
Image distribution after data enhancement.

Magnification times	Training set	Test set
50X	16572	624
100X	16931	609
200X	17003	535
400X	15604	572
Aggregate	66110	2340

During the experiments, all training data are resized to 224 × 224× 1, then divided into mini-batches, with each mini-batch containing 32 images. The Adam optimizer is employed as the optimizer for this experiment, automatically adjusting the learning rate during training to enhance the model's classification accuracy. The parameters of the Adam optimizer are set to default values.

For the loss function, this study uses the Focal Loss function. ReLU functions are employed as activation functions during training.

2.6. Focal loss function

In typical classification tasks, the cross-entropy function is commonly used as the loss function. For binary classification, the formula for Binary Cross-Entropy (BCE), shown in Equation (3), is used:

$$\mathrm{Loss} = -y\log\hat{y} - (1-y)\log(1-\hat{y}) \tag{3}$$

Here, *Loss* represents the loss value, y is the pathological label (where $y = 0$ represents benign and $y = 1$ represents malignant), and $\hat{y} \in (0, 1)$ is the predicted value from the neural network.

While the cross-entropy function has widespread use, it has a notable limitation. It can be influenced by easily classified samples, leading to deviations from the correct optimization direction during training, which can impact classification performance. As shown in Table 1, our dataset exhibits class imbalance issues. After data augmentation, the training set contains 20,856 images of benign tumors and 45,588 images of malignant tumors, indicating a significant disparity between the two categories. To address this, the focal loss function is employed as a replacement for the binary cross-entropy function. Its formula (Equation (4)) is as follows:

$$\mathrm{L_{fl}} = -\mathrm{a}(1-\hat{y})^{\beta} y\log\hat{y} - (1-\alpha)\hat{y}^{\beta}(1-y)\log-\hat{y}\Big) \tag{4}$$

In this equation, L_{fl} represents the loss value for the focal loss function,

and α and β are introduced hyperparameters, typically set to 0.25 and 2, respectively. Experimental results demonstrate that incorporating the focal loss function helps alleviate class imbalance issues to some extent and enhances the model's classification performance.

3. Results and discussion

3.1. Evaluation metrics

Medical image classification is typically evaluated from two perspectives: patient-level and image-level.

In this study, patient-level evaluation is not considered, and only image-level classification performance is assessed. The image-level recognition rate, denoted as "Image Recognition Rate," can be calculated using Equation (5):

$$\text{Image Recognition Rate} = \frac{N_r}{N_{all}} \tag{5}$$

Where:

N_{all} represents the total number of mammography Images in the test set.

N_r represents the number of images that were correctly classified.

This metric measures the accuracy of the model in classifying individual images.

3.2. Comparison of accuracy under different loss functions

In this experiment, the focal loss function (Focal Loss) is compared to the widely used binary cross-entropy (BCE) in classification tasks. These two functions are employed as the loss functions during training, and the experimental results are presented in Table 3. The observations from Table 3 are as follows.

(1) When using the Focal Loss as the loss function, the classification accuracy for benign and malignant tumors differs by only 0.59%. In contrast, when using BCE, the difference is 4.54%. In the BCE case, the model exhibits a bias towards the majority class (malignant tumors), which is not conducive to tumor diagnosis.
(2) When the Focal Loss is employed, although the classification accuracy for malignant tumors is slightly lower compared to using BCE, there is a significant improvement in the accuracy of benign tumor classification. Such a model is closer to real-life scenarios and exhibits greater robustness.
(3) The model's overall average accuracy is improved when using the Focal Loss.

These results highlight the advantages of using the Focal Loss function, particularly in addressing class imbalance and improving the overall performance of the model in medical image classification.

3.3. Comparison of accuracy under different training strategies

In this experiment, four different training strategies were employed, each utilizing the Focal Loss as the loss function. These strategies included data augmentation combined with transfer learning, data augmentation alone, transfer learning alone, and a strategy involving neither data augmentation nor transfer learning. The results, presented in Fig. 4, showcase the accuracy of the best model on the test set after 10,000 network training iterations for each strategy. This comparative analysis helps assess the impact of different training approaches on the model's classification performance.

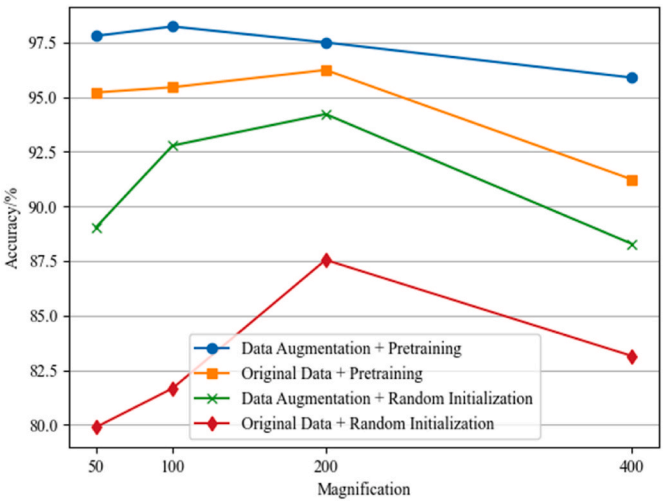

Fig. 4. Accuracy under four training strategies.

As depicted in Fig. 4, the adoption of transfer learning strategies, with or without data augmentation, resulted in a substantial improvement in accuracy (as seen in the orange and blue curves in Fig. 4). This confirms the effectiveness of transfer learning strategies. When data augmentation strategies were employed, whether or not transfer learning was used for network initialization, there was a noticeable improvement in training accuracy (as evident in the blue and green curves in Fig. 4), validating the effectiveness of data augmentation strategies. These experiments demonstrate that the effective training strategies employed in this study mitigate overfitting during training and significantly enhance the model's generalization capabilities, achieving recognition rates ranging from 95% to 98% on the dataset.

3.4. Comparison with other classification methods

To better evaluate the performance of this study's model, a comparison was made with other classification methods applied to the same dataset. These methods were evaluated using the same criteria, where image-level recognition rate serves as the benchmark (as shown in Table 4). The comparison demonstrates that the recognition accuracy of this study's method for all four different magnification levels surpasses that of other classification methods. This underscores the effectiveness of the training strategies used in this study and the robustness of the deep learning model developed herein.

Furthermore, the deep learning technology applied in this paper has been tested to be robust and reliable, and may even be extended to more fields of applications related to machine intelligence (Wong, 2023), which may include industrial implementations of smart diagnostics in the manufacturing sector (Liu et al., 2024; Zhou, Du, Liu, & Shen, 2024) as an example.

Table 3
Comparison of accuracy with different loss functions.

Loss function	Healthy	Cancer	Average accuracy
BCE	92.79	97.33	95.06
Focal Loss	96.65	97.24	96.945

Table 4
Comparison of recognition accuracy of various methods with different magnifications.

Algorithm	50X	100X	200X	400X
AlexNet network	87.36	84.40	85.25	82.55
VGG network + Transfer learning	86.54	87.31	86.02	83.10
GooleNet + Transfer learning	92.49	91.90	91.27	89.93
Proposed method	**97.71**	**97.87**	**96.54**	**94.20**

4. Conclusion

To address the limitations of traditional machine learning in breast cancer histopathology image classification and improve classification accuracy, this paper introduces a CNN-based breast cancer histopathology image classification model. The model is trained and optimized on our dataset, achieving an average recognition rate of 96.945% across four different magnification levels. Notably, recognition rates exceed 95.5% for the 50X, 100X, and 200× magnification levels, demonstrating excellent classification capabilities.

To tackle the challenge of limited medical image datasets, this study employs transfer learning and data augmentation strategies. Transfer learning initializes the network, and data augmentation expands the dataset to twelve times its original size, mitigating the risk of overfitting. Additionally, to address class imbalance issues in the dataset, this paper utilizes the focal loss function instead of traditional cross-entropy loss. Through various comparative experiments, the paper validates the excellence of the proposed model and the effectiveness of its training strategies, offering valuable guidance for early breast cancer detection and diagnosis.

Ethical approval

All human subjects in this study have given their written consent for the participation of our research.

Declaration of Competing interest

The authors declare that there is no conflict of interest.

Acknowledgment

N. A.

References

LeCun, Y., Bengio, Y., & Hinton, G. (2015). Deep learning. *Nature: International Weekly Journal of Science, 521*(7553), 436–444.

Molin Liu, Lv, Jun, Shichang Du, Yafei Deng, Shen, Xiaoxiao, & Yulu Zhou. (2024) , Multi-resource constrained flexible job shop scheduling problem with fixture-pallet combinatorial optimisation. Computers & Industrial Engineering, 188, 109903.

Nawaz, M., Adel, A., & Hassan, T. S. (2018). Multiclass breast cancer classification using deep learning convolutional neural network. *International Journal of Advanced Computer Science and Applications, 9*(6), 316–332.

Roy, S. D., Das, S., Devroop, K., et al. (2021). Computer aided breast cancer detection using ensembling of texture and statistical image features. *Sensors, 21*(11), 3628.

Russakovsky, O., Deng, J., Su, H., et al. (2015). ImageNet large scale visual recognition challenge. *International Journal of Computer Vision, 115*(3), 211–252.

Shi, J., Ye, Y., Zhu, D., Su, L., Huang, Y., & Huang, J. (2021a). Comparative analysis of pulmonary nodules segmentation using multiscale residual U-Net and fuzzy C-means clustering, Comput. *Methods Programs Biomed, 209*, Article 106332.

Shi, J., Ye, Y., Zhu, D., Su, L., Huang, Y., & Huang, J. (2021b). Super-resolution reconstruction of pneumocystis carinii pneumonia images based on generative confrontation network. *215*, Article 106578.

Simonyan, K., & Zisserman, A. (2014). *Very deep convolutional networks for large-scale image recognition*. arXiv preprint arXiv:1409.1556.

Spanhol, F. A., Oliveira, L. S., Petitjean, C., et al. (2016a). A dataset for breast cancer histopathological image classification. *IEEE Transactions on Biomedical Engineering, 63*(7), 1455–1462.

Spanhol, F. A., Oliveira, L. S., Petitjean, C., et al. (2016b). Breast cancer histopathological image classification using Convolutional Neural Networks. In *International joint conference on neural networks (IJCNN)* (pp. 2560–2567).

Weiss, K., Khoshgoftaar, T. M., & Wang, D. D. (2016). A survey of transfer learning. *Journal of Big Data, 3*(1), 9.

Wild, C. P., Weiderpass, E., & Stewart, B. W. (2020). *World cancer report: Cancer research for cancer prevention*. Lyon: International Agency for Research on Cancer.

Wong, K. K. L. (2023). *Cybernetical Intelligence: Engineering Cybernetics with Machine Intelligence*. Hoboken, New Jersey: John Wiley & Sons, Inc.

Wong, K. K. L., Fortino, G., & Abbott, D. (2020). Deep learning-based cardiovascular image diagnosis: A promising challenge. *Future Generation Computer Systems, 110*, 802–811.

Wong, K. K. L., Sun, Z., Tu, J. Y., Worthley, S. G., Mazumdar, J., & Abbott, D. (2012). Medical image diagnostics based on computer-aided flow analysis using magnetic resonance images. *Computerized Medical Imaging and Graphics, 36*(7), 527–541.

Wong, K. K. L., Zhang A, A., & Yang, K. (2022). GCW-UNet segmentation of cardiac magnetic resonance images for evaluation of left atrial enlargement. *Computer Methods and Programs in Biomedicine*, Article 106915.

Ye, Y., Shi, J., Huang, Y., Zhu, D., Su, L., & Huang, J. (2021). Management of medical and health big data based on integrated learning-based health care system: A review and comparative analysis. *Computer Methods and Programs in Biomedicine, 209*, Article 106293.

Zhao, C., Du, S., Lv, J., Deng, Y., & Li, G. (2023). A novel parallel classification network for classifying three-dimensional surface with point cloud data. *Journal of Intelligent Manufacturing, 34*(2), 515–527.

Zhu, X., Wei, Y., Lu, Y., Zhao, M., Yang, K., Wu, S., … Wong, K. K. L. (2020). Comparative analysis of active contour and convolutional neural network in rapid left-ventricle volume quantification using echocardiographic imaging. *Computer Methods and Programs in Biomedicine, 199*, 105914.

Zhou, Y., Du, S., Liu, M., & Shen, X. (2024). Machine-fixture-pallet resources constrained flexible job shop scheduling considering loading and unloading times under pallet automation system. *Journal of Manufacturing Systems, 73*, 143–158.

Zou, W., Lu, H., & Ye, M. (2020). Breast cancer histopathological image classification based on convolutional neural networks. *Computer Engineering and Design, 41*(6), 1749–1754.